Fluctuations and correlations in high temperature QCD

R. Bellwied, S. Borsányi, Z. Fodor, S. D. Katz, A. Pásztor, C. Ratti, and K. K. Szabó

Fluctuations and correlations in high temperature QCD

R. Bellwied[5], S. Borsanyi[1], Z. Fodor[1,2,3], S. D. Katz[2,4], A. Pásztor[1], C. Ratti[5], K. K. Szabo[1,3]

[1] *Department of Physics, Wuppertal University,*
Gaussstr. 20, D-42119 Wuppertal, Germany
[2] *Inst. for Theoretical Physics, Eötvös University,*
Pázmány P. sétány 1/A, H-1117 Budapest, Hungary
[3] *Jülich Supercomputing Centre,*
Forschungszentrum Jülich, D-52425 Jülich, Germany
[4] *MTA-ELTE "Lendület" Lattice Gauge Theory Research Group,*
Pázmány P. sétány 1/A, H-1117 Budapest, Hungary
[5] *Department of Physics, University of Houston, Houston, TX 77204, USA*

We calculate second- and fourth-order cumulants of conserved charges in a temperature range stretching from the QCD transition region towards the realm of (resummed) perturbation theory. We perform lattice simulations with staggered quarks; the continuum extrapolation is based on $N_t = 10 \ldots 24$ in the crossover-region and $N_t = 8 \ldots 16$ at higher temperatures. We find that the Hadron Resonance Gas model predictions describe the lattice data rather well in the confined phase. At high temperatures (above $\sim$250 MeV) we find agreement with the three-loop Hard Thermal Loop results.

I. INTRODUCTION

The Quark Gluon Plasma was formed in the Early Universe just a few microseconds after the Big Bang; today it is produced in heavy ion collision experiments at the Large Hadron Collider (LHC) at CERN and the Relativistic Heavy Ion Collider (RHIC) at Brookhaven Lab (BNL). This phase exists at high temperatures and/or densities, and is separated from the hadronic phase of Quantum Chromodynamics (QCD) by a cross-over transition [1]. Lattice QCD has determined the temperature of this cross-over in Refs. [2–5].

Below the transition temperature, the thermodynamics is governed by massive hadrons with integer charges, whereas at high temperature nearly free and nearly massless quarks with fractional charges and gluons dominate. Fluctuations of various conserved charges are sensitive probes of the quantum numbers and the associated masses, and have been proposed as a signal of the deconfinement transition [6, 7]. In heavy ion experiments there is an ongoing effort to measure the moments of conserved charge distributions [8], which can be related one-to-one to fluctuations. They are particularly interesting for the beam energy scan program at RHIC, since they may signal a nearby critical end point: higher order moments of net proton distributions are sensitive to an increase in the correlation length [9]. Fluctuations can also be used to extract the chemical freeze-out temperature and chemical potential [10], as an alternative method to the thermal fits to particle yields or ratios [11–15]. The STAR collaboration has published the first four moments of the net-proton [16] and net-electric charge [17] distributions. In parallel to the experimental efforts, the past years have witnessed a rapid development in the lattice calculations of fluctuations [18, 19], leading to quantitative estimates of the chemical freeze-out temperature and chemical potential for a range of RHIC energies [20].

Diagonal quark number susceptibilities have already been calculated in the early dynamical simulations [21–23]; these were later complemented by the off-diagonal ones [24–29]. In the following years, higher order fluctuations have been calculated up to the sixth order [29, 30], with the main motivation to extrapolate several thermodynamic observables to larger values of the chemical potential. These were staggered simulations projects, but studies with Wilson quarks are also emerging [31–35]. Strangeness fluctuations were used also to locate the transition temperature and, for this purpose, they were continuum extrapolated. With Wilson quarks this was done with pion masses down to 285 MeV [31, 32], for staggered quarks the continuum limit was calculated at the physical point [2–4, 36]. Continuum results for the other second cumulants appeared first in Ref. [37] then in Ref. [36]. Selected higher order fluctuations were continuum extrapolated first in Refs. [19, 38–40].

Below the cross-over temperature, hadrons (mesons and baryons) dominate the thermodynamics. In this regime, the Hadron Resonance Gas (HRG) model provides a simple description of thermodynamic quantities, including specific fluctuations or correlations [41, 42]. Even before simulations with physical quark masses could be performed, lattice QCD data were well described by the HRG model if the actual particle spectrum was replaced by the unphysical one simulated on the lattice [43, 44]. The success of the HRG model based on the experimental resonance table has been demonstrated later in several papers with physical quark masses and continuum extrapolation for the chiral condensate [4], the equation of state [45] and fluctuations [36, 37].

The concept of HRG has motivated new studies where fluctuation-based observables were proposed for which, within the framework of the HRG model, only particles and resonances with a specific quantum number contribute (e.g. baryons in a specific strangeness sector) [46]. Since at low T most lattice results agree with the HRG predictions, which is no longer true in the deconfined phase, the highest temperature of agreement can be a model-dependent indicator of deconfinement, that can be studied on a flavor-specific basis [39].

Very high temperature QCD is best discussed in terms of improved perturbation theory. The QCD thermodynamic potential is known up to $\alpha^3 \log(\alpha)$ order [47]. This result was later generalized to finite chemical potentials [48] and the quark number susceptibilities were calculated to the same order [49]. The soft contributions to these unimproved perturbative results can be resummed via dimensional reduction [50]. This idea has been applied to the four-loop perturbative quark number susceptibilities [51, 52].

The hard thermal loop perturbation theory reorganizes the perturbative series, enhancing its convergence [53, 54]. Recently, the next-to-next-to-leading order pressure and energy density were calculated for the SU(3) theory, [55], dramatically improving the agreement with lattice simulations [56, 57]. Soon afterwards, the full QCD result was calculated, too [58, 59]. Fluctuations were calculated at one [51], two [60] and three loop order [61], improving the earlier HTL calculations of susceptibilities [62, 63]. This result was later generalized to finite chemical potentials [64].

In general, these highly resummed perturbative results are expected to provide a good approximation, but their range of validity can only be determined if they are compared with a non-perturbative approach, e.g. lattice QCD simulations. Such comparisons have already been made, first on the level of the equation of state [59]. Unfortunately, for this observable, the renormalization scale-dependence is too large for a definitive answer on the range of validity. Fluctuations, however, offer a more strict test for these diagrammatic approaches because of the rather small renormalization scale dependence of the result from dimensional reduction (DR) [52] and from hard thermal loops (HTL) [61]. Today lattice calculations at high temperatures are available e.g. with the HISQ action of the BNL-Bielefeld group [36, 40] and also with the 2stout action of the Wuppertal-Budapest collaboration [37, 38].

In this paper, we present results on diagonal and non-diagonal second and fourth order fluctuations, in a temperature range which stretches from the transition region to the perturbation theory domain. Our simulations are performed within the 2nd generation staggered thermodynamics program (4stout action). We start with the discussion of the conserved charges in the grand canonical field theory and provide details on how their fluctuations are calculated on the lattice. After describing our lattice thermodynamics program, the scale setting procedure and the finite temperature simulations, we highlight the technical challenges of a continuum extrapolation and the estimate of the systematic error on the continuum results. The results are organized in two sections. First we consider the cross-over region, around the point where the Hadron Resonance Gas loses its predictive power. Afterwards we compare our data to (resummed) perturbative results at high temperatures. We close with some concluding remarks pointing to further directions of research.

II. FLUCTUATIONS IN LATTICE QCD

A. QCD as a grand canonical ensemble

In a canonical ensemble, the conserved charges are external parameters. In a heavy ion collision, for example, the number of baryons, their electric charge and the vanishing strangeness are fixed during the entire collision, expansion of the plasma and freeze-out. A grand canonical ensemble emerges if a small sub-system is considered, that is still large enough to be close to the thermodynamic limit [65].

In QCD there exists a conserved charge for each quark flavor, thus one can introduce four quark chemical potentials in a $2 + 1 + 1$ flavor system: μ_u, μ_d, μ_s and μ_c, in short $\{\mu_q\}$.

The expectation number of a conserved charge is then found as a derivative with respect to the chemical potential.

$$\langle N_i \rangle = T \frac{\partial \log Z(T, V, \{\mu_i\})}{\partial \mu_i} \tag{1}$$

The response of the system to the thermodynamic force μ_i is proportional to the fluctuation of the conserved charge:

$$\frac{\partial \langle N_i \rangle}{\partial \mu_j} = T \frac{\partial^2 \log Z(T, V, \{\mu_q\})}{\partial \mu_j \partial \mu_i} = \frac{1}{T} (\langle N_i N_j \rangle - \langle N_i \rangle \langle N_j \rangle) \tag{2}$$

Since N_i is an extensive thermodynamic quantity and so is its μ-derivative, there the $O(V^2)$ contributions cancel in Eq. (2). Charge conjugation symmetry implies that, at $\mu_q \equiv 0$, the expectation value of any odd combination vanishes, e.g. the last term in Eq. (2). However, there is no such symmetry for different flavors, allowing e.g. for a $\langle N_u N_d \rangle$ correlator. The first perturbative diagram that contributes to the latter consists of two fermion loops, connected by three gluon lines [62].

The free energy density ($-T/V \log Z$) is proportional to the pressure in large volumes:

$$\frac{p}{T^4} = \frac{1}{VT^3} \log Z(T, V, \{\mu_q\}) . \tag{3}$$

The derivatives with respect to the chemical potential can thus be written in terms of the pressure:

$$\chi_{i,j,k,l}^{u,d,s,c} = \frac{\partial^{i+j+k+l}(p/T^4)}{(\partial \hat{\mu}_u)^i (\partial \hat{\mu}_d)^j (\partial \hat{\mu}_s)^k (\partial \hat{\mu}_c)^l} \tag{4}$$

with $\hat{\mu}_q = \mu_q/T$. This normalization ensures that the cumulants stay dimensionless, and become finite in the infinite volume and infinite temperature limit. In this normalization $\chi_1(T, \{\mu_q\})$ is the expected number of quarks of the given flavor in a volume T^{-3}.

The higher derivatives with respect to the same quark chemical potential correspond to the higher moments of that flavor:

$$\text{mean}: \ M \sim \chi_1 \quad \text{variance}: \ \sigma^2 \sim \chi_2$$
$$\text{skewness}: \ S \sim \chi_3/\chi_2^{3/2} \quad \text{kurtosis}: \ \kappa \sim \chi_4/\chi_2^2 . \tag{5}$$

In experiment, the net-charge distribution moments are measured, each carrying an unknown volume factor. A known caveat is the fluctuation of these volumes themselves. The study of these goes beyond the scope of this paper,

see [66, 67]. For a fixed volume, though, the unknown volume factor in the actual experiment can be simply cancelled out by forming ratios of cumulants of the same conserved charge:

$$S\sigma = \chi_3/\chi_2 \quad ; \quad \kappa\sigma^2 = \chi_4/\chi_2$$
$$M/\sigma^2 = \chi_1/\chi_2 \quad ; \quad S\sigma^3/M = \chi_3/\chi_1 \, . \tag{6}$$

Phenomenological models and experiments usually work in the baryon number (B) - electric charge (Q) - strangeness (S) basis. Since the charm quark plays a negligible role in the transition region one can express these directions in the μ space as a three-dimensional transformation:

$$\mu_u = \frac{1}{3}\mu_B + \frac{2}{3}\mu_Q \, , \tag{7}$$

$$\mu_d = \frac{1}{3}\mu_B - \frac{1}{3}\mu_Q \, , \tag{8}$$

$$\mu_s = \frac{1}{3}\mu_B - \frac{1}{3}\mu_Q - \mu_S \, . \tag{9}$$

The fluctuations of the conserved charges $(B, Q$ and $S)$ can then be expressed in terms of the quark derivatives. In addition, the (z component of the) light isospin is often studied with $\mu_I = (\mu_u - \mu_d)$. Assuming zero chemical potential and degenerate u and d quarks on the lattice, several simplifications occur, and we have [27, 36]:

$$\chi_2^B = \frac{1}{9}\left[2\chi_2^u + \chi_2^s + 4\chi_{11}^{us} + 2\chi_{11}^{ud}\right] \, , \tag{10}$$

$$\chi_2^Q = \frac{1}{9}\left[5\chi_2^u + \chi_2^s - 2\chi_{11}^{us} - 4\chi_{11}^{ud}\right] \, , \tag{11}$$

$$\chi_2^I = \frac{1}{2}\left[\chi_2^u - \chi_{11}^{ud}\right] \, , \tag{12}$$

$$\chi_{11}^{BQ} = \frac{1}{9}\left[\chi_2^u - \chi_2^s - \chi_{11}^{us} + \chi_{11}^{ud}\right] \, , \tag{13}$$

$$\chi_{11}^{BS} = -\frac{1}{3}\left[\chi_2^s + 2\chi_{11}^{us}\right] \, , \tag{14}$$

$$\chi_{11}^{QS} = \frac{1}{3}\left[\chi_2^s - \chi_{11}^{us}\right] \, . \tag{15}$$

Indeed, due to the $u \leftrightarrow d$ degeneracy the six second order combinations in the B, Q, S space can be expressed in terms of four quark correlators. Inverting Eqs. (10-15) one finds the quark-flavor derivatives from the fluctuations in the phenomenological basis. These can be used to translate the results from the Hadron Resonance Gas model.

$$\chi_2^u = 2\chi_2^B + \chi_2^Q + \chi_{11}^{BS} \, , \tag{16}$$

$$\chi_2^s = \chi_2^S \, , \tag{17}$$

$$\chi_{11}^{ud} = \frac{5}{2}\chi_2^B - \chi_2^Q + \frac{1}{2}\chi_2^S + 2\chi_{11}^{BS} \, , \tag{18}$$

$$\chi_{11}^{us} = -\frac{1}{2}\chi_2^S - \frac{3}{2}\chi_{11}^{BS} = -3\chi_{11}^{QS} + \chi_2^S = \frac{3}{2}\chi_2^B - \frac{1}{2}\chi_2^S - 3\chi_{11}^{BQ} \, , \tag{19}$$

There are 15 fourth order correlators in the (B, Q, S) space that can be expressed in terms of 9 fourth order quark-correlators. The kurtosis of the baryon and the electric charge is given by the following correlators:

$$\chi_4^B = \tfrac{1}{81}\left[2\chi_4^u + \chi_4^s + 6\chi_{22}^{ud} + 12\chi_{22}^{us} + 8\chi_{13}^{us} + 8\chi_{31}^{us} + 8\chi_{31}^{ud} + 24\chi_{211}^{uds} + 12\chi_{112}^{uds}\right] \, , \tag{20}$$

$$\chi_4^Q = \tfrac{1}{81}\left[17\chi_4^u + \chi_4^s + 24\chi_{22}^{ud} + 30\chi_{22}^{us} - 4\chi_{13}^{us} - 28\chi_{31}^{us} - 40\chi_{31}^{ud} + 24\chi_{211}^{uds} - 24\chi_{112}^{uds}\right] \, , \tag{21}$$

other, mixed derivatives can be calculated analogously.

Eqs. (20,21) refer to the charmless definition of the baryon number and the electric charge. In the phenomenologically relevant temperature region (up to 170 MeV) this simplification has no impact on the observables (e.g. χ_{11}^{BQ}). We stress that our variables still refer to exactly conserved charges. We will stick to the definition in Eqs. (10,20) also at higher temperatures, for the reason that the Hard Thermal Loop results refer to fluctuations of three light

baryons, and the heavy charm quark should not be counted in the comparison. If we do count the charm quarks the diagonal fluctuations will read:

$$\chi_2^{B,(n_f=4)} = \frac{1}{9} \left[2\chi_2^u + 2\chi_{11}^{ud} + 4\chi_{11}^{us} + 4\chi_{11}^{uc} + \chi_2^s + 2\chi_{11}^{sc} + \chi_2^c \right] , \tag{22}$$

$$\chi_2^{Q,(n_f=4)} = \frac{1}{9} \left[5\chi_2^u - 4\chi_{11}^{ud} - 2\chi_{11}^{us} + 4\chi_{11}^{uc} + \chi_2^s - 4\chi_{11}^{sc} + 4\chi_2^c \right] , \tag{23}$$

$$\chi_4^{B,(n_f=4)} = \frac{1}{81} \left[2\chi_4^u + 8\chi_{31}^{ud} + 8\chi_{31}^{us} + 8\chi_{31}^{uc} + 6\chi_{22}^{ud} + 24\chi_{211}^{uds} + 24\chi_{211}^{udc} + 12\chi_{22}^{us} + 24\chi_{211}^{usc} + 12\chi_{22}^{uc} + 12\chi_{112}^{uds} \right.$$
$$\left. + 24\chi_{1111}^{udsc} + 12\chi_{112}^{udc} + 8\chi_{13}^{us} + 24\chi_{121}^{usc} + 24\chi_{112}^{usc} + 8\chi_{13}^{uc} + \chi_4^s + 4\chi_{31}^{sc} + 6\chi_{22}^{sc} + 4\chi_{13}^{sc} + \chi_4^c \right] , \tag{24}$$

$$\chi_4^{Q,(n_f=4)} = \frac{1}{81} \left[17\chi_4^u - 40\chi_{31}^{ud} - 28\chi_{31}^{us} + 56\chi_{31}^{uc} + 24\chi_{22}^{ud} + 24\chi_{211}^{uds} - 48\chi_{211}^{udc} + 30\chi_{22}^{us} - 120\chi_{211}^{usc} + 120\chi_{22}^{uc} - 24\chi_{112}^{uds} \right.$$
$$\left. + 96\chi_{1111}^{udsc} - 96\chi_{112}^{udc} - 4\chi_{13}^{us} + 24\chi_{121}^{usc} - 48\chi_{112}^{usc} + 32\chi_{13}^{uc} + \chi_4^s - 8\chi_{31}^{sc} + 24\chi_{22}^{sc} - 32\chi_{13}^{sc} + 16\chi_4^c \right] . \tag{25}$$

At high temperature, fluctuations approach the Stefan-Boltzmann limit. For an ideal gas, the pressure at finite chemical potential reads [68, 69]

$$\frac{p}{T^4} = \frac{8\pi^2}{45} + \frac{7\pi^2}{60} N_f + \frac{1}{2} \sum_f \left(\frac{\mu_f^2}{T^2} + \frac{\mu_f^4}{2\pi^2 T^4} \right) . \tag{26}$$

For the second and fourth order fluctuations this means that in the high temperature limit $\chi_2 \to 1$ and $\chi_4 \to 6/\pi^2$, and no mixed derivatives survive.

B. Fluctuations on the lattice

The standard way to introduce the chemical potential on the lattice is to modify the temporal links, like the A_4 component of a homogeneous U(1) field [70]:

$$U_4(\mu) = e^\mu U_4, \quad U_4^+(\mu) = e^{-\mu} U_4^+ \tag{27}$$

The fermion matrix M is built from the μ-dependent links. In the staggered formalism, which we will use in this paper, each fermion flavor may carry an independent chemical potential. The fermion determinants express a single quark flavor.

$$Z = \int \mathcal{D}U \ e^{-S_g} (\det M_u)^{1/4} (\det M_d)^{1/4} (\det M_s)^{1/4} (\det M_c)^{1/4} , \tag{28}$$

where S_g is the gauge action. To be specific, in this paper we use the tree-level Symanzik improvement in S_g, however its form plays no role in the fluctuation-related formulas. The derivative of the staggered fermion matrix M takes the following from:

$$\frac{dM}{d\mu} \psi(x) = \frac{1}{2} \eta_4(x) \left[U_4(x)\psi(x+\hat{4}) + U_4^+(x-\hat{0})\psi(x-\hat{4}) \right] ,$$

$$\frac{d^2M}{d\mu^2} \psi(x) = \frac{1}{2} \eta_0(x) \left[U_4(x)\psi(x+\hat{4}) - U_4^+(x-\hat{0})\psi(x-\hat{4}) \right] ;$$

any higher odd derivative is equal to $dM/d\mu$, while any higher even derivative is equal to $d^2M/d\mu^2$. $\eta_\nu(x)$ is the Kogut-Susskind phase factor.

For the fourth order μ-derivative one has to evaluate the fourth derivatives of det M. These are traces of the fermion matrix that have to be calculated for every generated finite temperature configuration [26]:

$$A_j = \frac{d}{d\mu_j} \log(\det M_j)^{1/4} = \frac{1}{4} \text{tr} M_j^{-1} M_j' , \tag{29}$$

$$B_j = \frac{d^2}{(d\mu_j)^2} \log(\det M_j)^{1/4} = \frac{1}{4} \text{tr} \left(M_j'' M_j^{-1} - M_j' M_j^{-1} M_j' M_j^{-1} \right) , \tag{30}$$

$$C_j = \frac{d^3}{(d\mu_j)^3} \log(\det M_j)^{1/4} = \frac{1}{4} \text{tr} \left(M_j' M_j^{-1} - 3M_j'' M_j^{-1} M_j' M_j^{-1} \right.$$
$$\left. + 2M_j' M_j^{-1} M_j' M_j^{-1} M_j' M_j^{-1} \right) , \tag{31}$$

$$D_j = \frac{d^4}{(d\mu_j)^4} \log(\det M_j)^{1/4} = \frac{1}{4}\mathrm{tr}\left(M_j'' M_j^{-1} - 4M_j' M_j^{-1} M_j' M_j^{-1} - 3M_j'' M_j^{-1} M_j'' M_j^{-1}\right.$$
$$+12 M_j'' M_j^{-1} M_j' M_j^{-1} M_j' M_j^{-1}$$
$$\left.-6 M_j' M_j^{-1} M_j' M_j^{-1} M_j' M_j^{-1} M_j' M_j^{-1}\right), \tag{32}$$

Using the simple notation ∂_j for $\partial/\partial\mu_j$, the derivatives can now be written for the full free energy:

$$\partial_i \log Z = \langle A_i \rangle. \tag{33}$$

The derivative of the expectation value of any X lattice observable is obtained as

$$\partial_j \langle X \rangle = \langle X A_j \rangle - \langle X \rangle \langle A_j \rangle + \langle \partial_j X \rangle. \tag{34}$$

When we derive the higher order formulas (see also [26]) we assume non-zero chemical potential and use Eq. 34 recursively. Setting in the end $\mu = 0$ we have, to second order,

$$\partial_i \partial_j \log Z = \langle A_i A_j \rangle - \langle A_i \rangle \langle A_j \rangle + \delta_{ij} \langle B_i \rangle, \tag{35}$$

and to fourth order, exploiting the degeneracy between the light quark flavors:

$$\partial_i^4 \log Z = \langle A_i^4 \rangle - 3\langle A_i^2 \rangle^2 + 3\left(\langle B_i^2 \rangle - \langle B_i \rangle^2\right)$$
$$+6\left(\langle A_i^2 B_i \rangle - \langle A_i^2 \rangle \langle B_i \rangle\right) + 4\langle A_i C_i \rangle + \langle D_i \rangle, \tag{36}$$

$$\partial_u^3 \partial_d \log Z = \langle A_u^4 \rangle - 3\langle A_u^2 \rangle^2$$
$$+3\left(\langle A_i^2 B_i \rangle - \langle A_i^2 \rangle \langle B_i \rangle\right) + \langle A_i C_i \rangle \tag{37}$$

$$\partial_u^2 \partial_d^2 \log Z = \langle A_u^4 \rangle - 3\langle A_u^2 \rangle^2 + \langle B_u^2 \rangle - \langle B_u \rangle^2$$
$$+2\left(\langle A_i^2 B_i \rangle - \langle A_i^2 \rangle \langle B_i \rangle\right) \tag{38}$$

$$\partial_u^2 \partial_s^2 \log Z = \langle A_u^2 A_s^2 \rangle - 2\langle A_u A_s \rangle^2 - \langle A_u^2 \rangle \langle A_s^2 \rangle + \langle B_u B_s \rangle - \langle B_u \rangle \langle B_s \rangle$$
$$+\langle A_u^2 B_s \rangle - \langle A_u^2 \rangle \langle B_s \rangle + \langle A_s^2 B_u \rangle - \langle A_s^2 \rangle \langle B_u \rangle \tag{39}$$

$$\partial_u^3 \partial_s \log Z = \langle A_u^3 A_s \rangle - 3\langle A_u^2 \rangle \langle A_u A_s \rangle$$
$$+3\left(\langle A_u A_s B_u \rangle - \langle A_u A_s \rangle \langle B_u \rangle\right) + \langle A_s C_u \rangle \tag{40}$$

$$\partial_u \partial_s^3 \log Z = \langle A_u A_s^3 \rangle - 3\langle A_s^2 \rangle \langle A_u A_s \rangle$$
$$+3\left(\langle A_u A_s B_s \rangle - \langle A_u A_s \rangle \langle B_s \rangle\right) + \langle A_u C_s \rangle \tag{41}$$

$$\partial_u \partial_d \partial_s^2 \log Z = \langle A_u^2 A_s^2 \rangle - 2\langle A_u A_s \rangle^2 - \langle A_u^2 \rangle \langle A_s^2 \rangle$$
$$+\langle A_u^2 B_s \rangle - \langle A_u^2 \rangle \langle B_s \rangle \tag{42}$$

$$\partial_u^2 \partial_d \partial_s \log Z = \langle A_u^3 A_s \rangle - 3\langle A_u A_s \rangle \langle A_u^2 \rangle$$
$$+\langle A_u A_s B_u \rangle - \langle A_u A_s \rangle \langle B_u \rangle. \tag{43}$$

We follow the standard stochastic strategy to calculate the traces $A \ldots D$, and evaluate them with a large number of Gaussian random sources. If one is only interested in up to the fourth derivative, five calls to the linear solver $Mx = b$ are necessary for each random source. Since the operator D appears only in connected contributions, we do not need it to high accuracy. A, on the other hand, appears in the disconnected term with the most difficult cancellation, so it needs to be evaluated more often. A requires one solver, while C requires three solvers. Thus, if we evaluate D with N sources, we evaluate the A operator $8N$ times and the B and C operators $4N$ times.

It was pointed out in [26] that, when products of traces are calculated (e.g. $\langle AA \rangle \sim \chi_2^{ud}$), the two (or more) operators in the product must be calculated with different (or uncorrelated) random sources. For this reason, we always use quartets of independent sources. We typically use $N = 128$ quartets in our analysis. Multi-right-hand-side solvers are particularly useful in this context, since these typically achieve a higher flop rate on many supercomputers, because the gauge fields do not have to be loaded from the memory with each source [71].

The numerical evaluation of these diagrams with multiple random sources can be accelerated by various means. One observation was that e.g. the A operator can be split into two parts $A_0 + \delta A$, where A_0 is the result of a truncated solver and δA is the difference between the truncated result and the full precision solution. The advantage is that δA can be evaluated with less sources, while the more noisy A_0 is cheaper to work with [72].
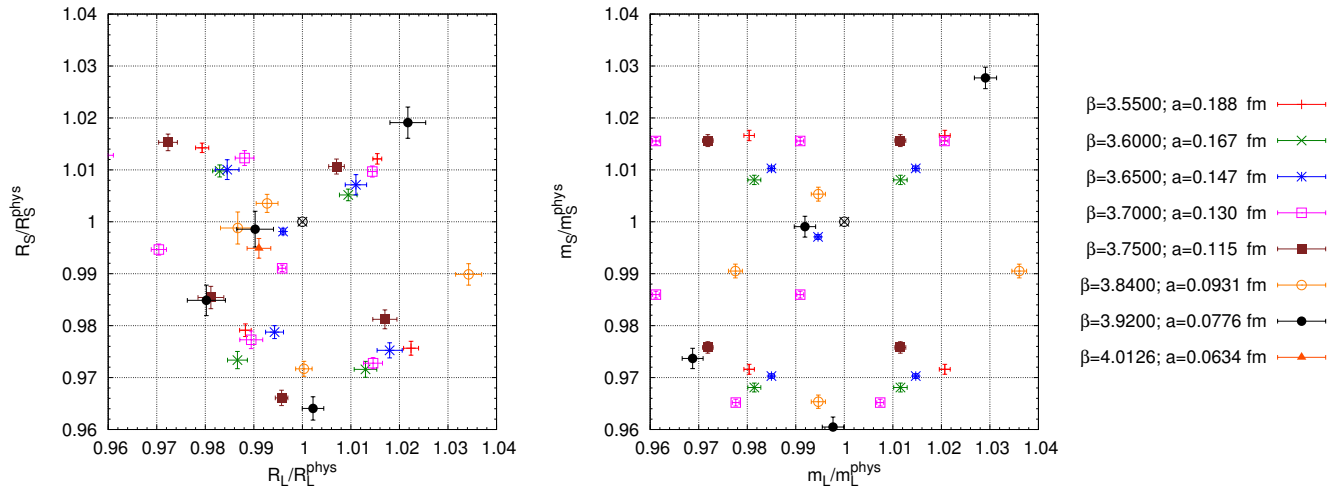
FIG. 1. Summary of our large volume zero temperature runs. The left panel shows the combinations in Eq. (44) where $R_S/R_S^{\text{phys}} = 1$ and $R_L/R_L^{\text{phys}} = 1$ define the physical point. We determine the physical bare quark masses by interpolating the bare parameters to precisely restore the R_S and R_L ratios (see Ref. [77] for details). The right panel shows the bare parameters rescaled by the interpolated quark mass. The errors on the rescaled run parameters come solely from the errors of the interpolation.

III. LATTICE ACTION AND ENSEMBLES

This work is part of the second generation thermodynamics program of the Wuppertal-Budapest collaboration. We use the tree-level Symanzik gauge action with 2+1+1 flavors of four times stout smeared staggered quarks [73], with the smearing parameter $\rho = 0.125$.

A. Zero temperature simulations and the line of constant physics

An essential step, before thermodynamics runs can be started with a new action, is the tuning of the mass parameters and the determination of the scale or, in other words, the mass and coupling renormalization of the theory for each lattice cut-off that the thermodynamics project intends to use. In this project we use degenerate up and down quarks. For simplicity, we do not tune the charm mass separately but accept the continuum extrapolated quark mass ratio $m_c/m_s = 11.85$ of Ref. [74]. The light and strange quark masses are obtained by tuning the following ratios to their physical values:

$$R_S^{\text{phys}} = \frac{2m_K^2 - m_\pi^2}{f_\pi^2} = 27.65, \quad R_L^{\text{phys}} = \frac{m_\pi}{f_\pi} = 1.069 \tag{44}$$

where we use the isospin-averaged pion and kaon masses (m_π and m_K) [75]. $f_\pi = 130.41$ MeV (see Ref. [76]) is used to set the scale.

In this work we use the zero temperature lattice configurations produced for the 4stout $T = 0$ project [77]. In the lattice spacing range $a = 0.188$ fm ... 0.077 fm we simulate four or more ensembles for eight inverse bare couplings $\beta = 6/g^2$. The RHMC streams for the ensembles are typically ~ 2000 trajectories long after thermalization. We parametrized these ensembles such that they form a $\pm 3\%$ bracket around the physical point, which is defined in Eq. (44). The box size of these zero temperature simulations was without exception $Lm_\pi \gtrsim 4$.

In Fig. 1 we summarize the zero temperature configurations. For each β we interpolated in the space of bare quark masses, getting these to a few per mill accuracy. On the left panel of Fig. 1 we show the combinations in Eq. (44). The right panel shows the position of individual bare parameters relative to the thus interpolated physical point (with details given in Ref. [77]).

Our finest large volume ensemble was simulated at $\beta = 4.0126$ on a $96^3 \times 144$ lattice. Its parameters were extrapolated and then corrected using simulations at this β in the flavor symmetric point, where all three light quark masses are degenerate (the charm mass staying physical).
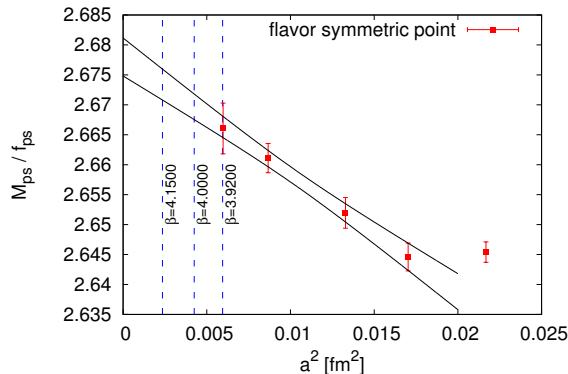
FIG. 2. Using the bare parameters calculated from the 2+1+1 theory's quark masses $\bar{m} = \frac{1}{3}(m_u + m_d + m_s)$, $m_c = 33.15\bar{m}$, we find a mild a^2 dependence for the pseudo-scalar mass-to-decay-constant ratio in the 3+1 flavor (flavor symmetric) theory. The matching bare mass $\bar{m}$ at larger β (finer lattice) can be determined at lower computational costs with 3+1 flavors. From $\bar{m}$, the bare masses of the 2+1+1 theory can be estimated.

The tuning effort using the flavor symmetric lattices goes as follows: first, we have to acknowledge that various scale setting schemes differ in the cut-off effects. Thus, changing the scale setting or tuning principle may introduce different cut-off effects on different parts of the line of constant physics. A continuum extrapolation that spans a larger range of lattice spacings will thus be distorted. To prevent this from happening, we match not only the scale but also the a^2 corrections and check for the insignificance of the a^4 effects whenever we are forced to switch between scale setting schemes along the line of constant physics. In this particular case, we chose the mass-independent renormalization scheme. For a fixed gauge coupling, we define a 3+1 flavor theory with the bare masses calculated from the ones of the 2+1+1 flavor theory: $\bar{m} = \frac{1}{3}(m_u + m_d + m_s)$, $m_c = 33.15\bar{m}$. This corresponds to a new scheme, and the pseudo-scalar mass to decay constant ratio will have an a^2 dependence. We plot this ratio in Fig. 2 (notice that, in the 2+1+1 theory, m_π/f_π had no a-dependence by definition). To extract the bare quark masses of the 2+1+1 dimensional theory at $\beta = 4.00$ and $\beta = 4.15$, we performed several simulations in the 3+1 flavor theory and interpolated $m_{\rm PS}/f_{\rm PS}$ in $\bar{m}$ to match the extrapolation in Fig. 2. We translated the masses back to the 2+1+1 flavor theory. At this point, we had to assume the $m_s/m_u = 27.63$ ratio, (which is consistent to our estimate from this work) [74, 78–80]. For the large volume simulation at $\beta = 4.0126$, which was running with such an indirectly tuned mass, we show the result in Fig. 1: the physical point is reproduced with an accuracy below one percent. The lattice spacings are shown in the plot, for the finest lattice we used the SU(2) low energy constants to extrapolate the final one percent to the physical point [81].

For even finer lattices we had to resort to a perturbative continuation of the line of constant physics. For the scale setting, the universal two-loop beta function does not yet describe the data. We have an alternative scale setting scheme w_0, introduced in [82], which is based on the gradient flow [83]. In that case, finite volume effects are small even for lattices as small as 1.5 fm [82]. This allowed to match again the value and a^2-dependence of w_0 at $\beta = 4.1479$ ($a \approx 0.047$ fm) and $\beta = 4.2562$ ($a \approx 0.038$ fm). The exploding autocorrelation times have forced us to use extremely long update streams (cca. 50000 trajectories) in a 40^4 volume. For even finer lattices we again measured and matched the flow and its leading lattice artefacts in fixed physical volume and topological sector in several subsequent steps. The final scale is plotted in Fig. 3. Since w_0 is of great interest for a wider community we will discuss its value, volume-dependence and other systematics in a publication devoted solely to scale setting.

Fig. 3 shows two versions of the scale setting. Controlled continuum extrapolations are independent of the choice of the scale setting scheme. The equivalence of the schemes on fine lattices is evident from Fig. 3. Nevertheless, this choice obviously influences the temperature of a particular ensemble. Especially for observables with large slope in temperature (e.g. the quark number susceptibilities in the cross-over region) the scale setting has an impact on the continuum scaling. We propagate this effect into the final error bars by calculating the continuum limits with both scale settings and include this in our study of systematics.
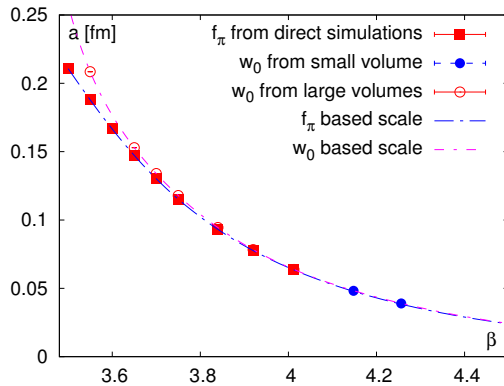
FIG. 3. The lattice spacing as a function of the inverse bare gauge coupling. The red squares show the outcome of the zero-temperature simulations with $Lm_\pi > 4$ for f_π. The scale in the w_0 scheme from the same runs is represented by the red circles. The blue dots correspond to smaller volumes, for which we used w_0 only. The differences coming from the two scale setting options are part of our systematic error estimate.

B. Finite temperature ensembles

We have generated three sets of ensembles, each with multiple lattice spacings and temperatures. In the first set we use the aspect ratio $LT = 3$, which might have finite volume effects, but gives a more favorable signal/noise ratio than larger volumes. The second set has $LT = 4$ and covers the entire transition range up to $2T_c$. Using these ensembles we can conclude that, wherever it was possible to perform a meaningful comparison (this includes all second order fluctuations and cross-correlators), finite volume effects on the $LT = 3$ ensembles are negligible for any lattice spacing, let alone in the continuum limit which is the largest source of systematic errors. We see significant finite volume effects only in the chiral condensate and susceptibility, which are not part of this study. For temperatures $T > 300$ MeV we do not keep the lattice geometry constant in our temperature scan, but keep the physical volume more-or-less constant with $LT_c \gtrsim 2$. For the finest, $N_t = 16$ lattices in this set we have thus used the lattices $80^3 \times 16$, $96^3 \times 16$, $112^3 \times 16$ and $128^3 \times 16$ for $T = 360, 440, 520$ and 600 MeV, respectively. In the high temperature range, the statistics is limited to ~ 1000 configuration / temperature / lattice spacing.

Table I shows the statistics for the $LT = 4$ ensembles in the cross-over region and in the quark gluon plasma phase. The temperatures below 150 MeV are used to compare the data to the predictions of the Hadron Resonance Gas model. The $LT = 3$ data set is restricted to the cross-over region (see table II). In the tables we give the number of configurations that we have analyzed for generalized quark number susceptibilities: these are separated by ten Rational Hybrid Monte Carlo (RHMC) trajectories. The acceptance range varies between 80 and 95%.

In the absence of visible finite volume effects in this range, we combine the results of these with the $LT = 4$ data set to enhance the signal. Indeed, the fluctuations of disconnected diagrams (especially $\langle A^4 \rangle - 3 \langle A^2 \rangle^2$) in Eq. (36) are heavily penalized by large volumes. This contribution also appears in the Taylor coefficients of the μ_B expansion and is the main source of noise.

C. Continuum extrapolation

The continuum extrapolation is mostly based on all available lattice spacings. Since fine lattices have lower statistics, the coarsest $N_t = 8$ results are usually included only in non-linear extrapolations, (e.g. $A + B/N_t^2 + C/N_t^4$ and other variations, where A is the continuum limit).

While for some observables (e.g. $\chi_2^S(T)$, $\chi_2^B(T)$) there is a clear range of safe linear extrapolation (in most cases $N_t \geq 10$), observables that are related to pion physics (e.g. $\chi_2^Q(T)$, $\chi_{11}^{ud}(T)$) show a very strong, non-linear $1/N_t^2$ dependence. Only for very fine lattices ($N_t \gtrsim 16$) we see a linear regime. Such behaviour have been already reported for the second order cumulants [36, 37].

Here we show the charge fourth and second moment for a single temperature in the confined phase ($T = 130$ MeV) in Fig. 4. This plot features an additional $96^3 \times 32$ point with 1485 analyzed configurations. We attempt several fit models, $f_1(N_t) = A + B\exp(-C/N_t^2)$ resembles a Boltzmann factor with an artefact mass vanishing as $1/N_t^2$. $f_2(N_t) = A + B/N_t^2 + C/N_t^2/\log(N_t)$ is similar to including a αa^2 term into the extrapolation. The shown continuum

T [MeV]	$32^3 \times 8$	$40^3 \times 10$	$48^3 \times 12$	$64^3 \times 16$	$80^3 \times 20$
125	10514	10080	10008	5027	2060
130	5766	4625	10253	5099	2000
135	14762	10590	10060	10189	2720
140	14863	5381	15043	4959	5097
145	5784	5020	10014	5019	1280
150	5464	5067	11043	5064	1631
153	4985	5517	6410	3641	-
155	5613	5001	10137	5015	1726
157	5526	5409	10018	5160	1065
160	5247	5017	4973	5073	1082
165	8169	10086	10496	5000	1000
170	6005	6113	5600	5111	600
175	12018	5375	5058	5104	972
180	5007	5089	5034	5013	1000
190	4900	5031	5121	5045	992
200	5989	5002	6722	1012	1000
220	5514	5000	7231	1003	1000
240	1712	5000	8082	3947	1000
250	10695	5685	5146	-	-
260	6287	5000	8623	5441	1000
270	11574	5682	5684	-	-
280	7067	5003	8751	1021	558
290	7316	5680	5684	-	-
300	5125	4917	5398	5310	1011

TABLE I. The statistics of lattices with $LT = 4$ aspect ratio. The numbers count the saved and analyzed configurations, each separated by ten RHMC updates.

T [MeV]	$24^3 \times 8$	$32^3 \times 10$	$40^3 \times 12$	$48^3 \times 16$	$64^3 \times 24$
130	39161	7736	10351	-	2007
135	41462	8724	10696	9892	3000
140	39867	8550	10240	8248	1551
145	40247	8518	10348	10130	2550
150	39996	8461	10569	6717	3044
155	19953	8625	10345	10211	1546
160	20015	9174	11611	10140	2063
165	10965	9750	10219	10136	1200

TABLE II. The number of analyzed configurations on lattices with $LT \approx 3$ aspect ratio. The configurations are separated by ten RHMC updates.

limit is based on the linear fit only. Taking these continuum extrapolations one has $\chi_4^Q/\chi_2^Q = 1.52(16)$, which compares to 1.62 in HRG. This particular ratio will be of direct phenomenological consequence, once the full temperature dependence is calculated from lattice QCD.

Not all observables require the finest lattices in our data set. Strange quark correlators receive no pion contributions, and the small relative taste violation in the kaon sector can be extrapolated away. We find that our data with its current precision allow linear fitting for $N_t \geq 10$. As examples we show the up-strange correlator (χ_{11}^{us}) and the higher order correlator between the same quarks χ_{22}^{us} in Fig. 5. Both have only disconnected contributions (see Eqs. (35,39)).

The parameters of the finite temperature runs have been tuned to have the same temperature in the f_π scale setting scheme. Since we also use the w_0 scale setting scheme, in that case the temperatures are no longer aligned and interpolations are necessary. The alignment of the temperatures is also not perfect in the f_π scale setting scheme,
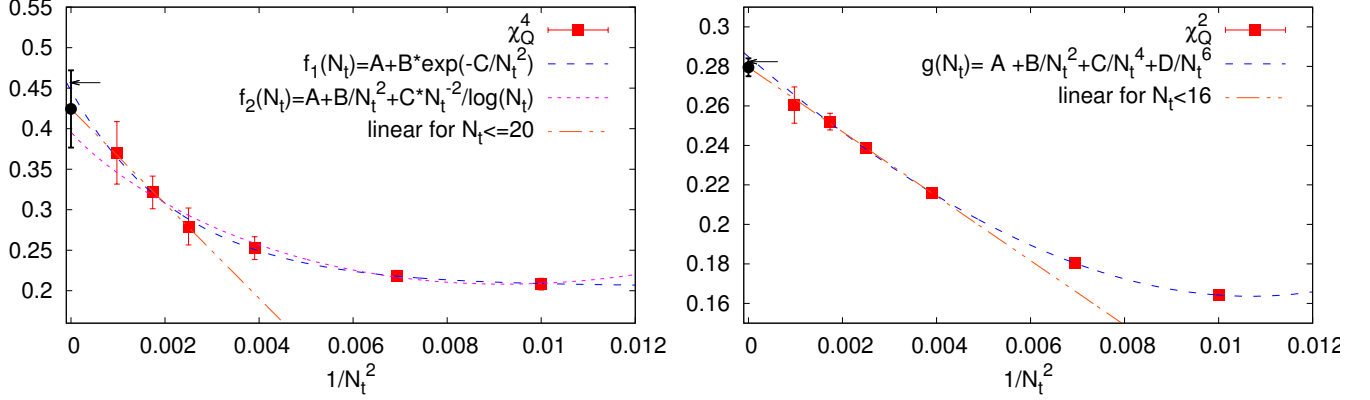
FIG. 4. Fluctuation data from the 4stout action at $T = 130$ MeV for a lattice resolution range $N_t = 10 \ldots 32$. This corresponds to the lattice spacings $a = 0.15 \ldots 0.047$ fm. A continuum extrapolation is possible by fitting sophisticated models but also via a simple linear fit through the finest lattices. The Hadron Resonance Gas model's prediction (small black arrows) is consistent with the continuum limit.
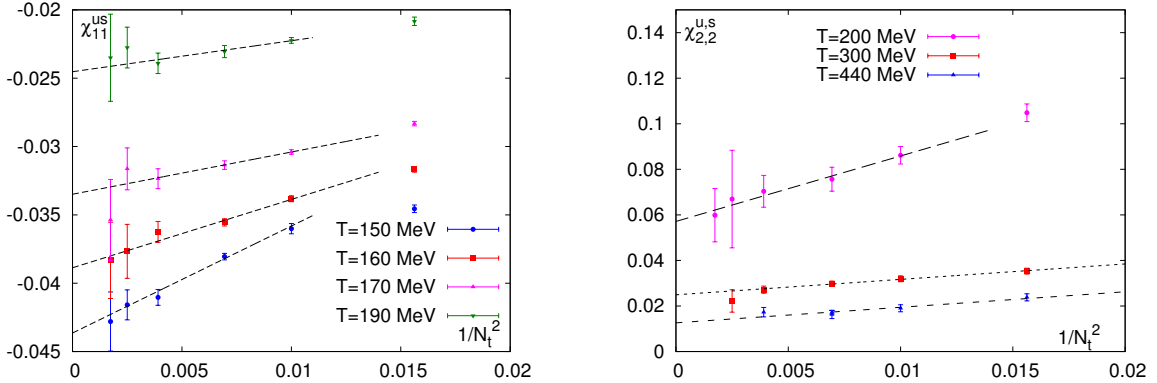

FIG. 5. Examples of linear continuum extrapolations for the light-strange correlators χ_{11}^{us} and χ_{22}^{us} at various temperatures. The error on our continuum results contains the systematics of varying the fit model, fit window, scale setting and interpolation, see text.

thus we interpolate all data sets. The interpolation is performed by fitting a spline through several (7-9) node points with two different sets of nodes so that the systematics of the interpolation can be picked up by the systematic error. We then perform the continuum extrapolation temperature by temperature, for those temperatures for which we had data points. The lattice artefacts of the diagonal fluctuations can be understood from tree-level perturbative diagrams [25]. We can correct for the α-independent part of the discretization errors by a T-independent factor (tree level improvement) [84]. This factor converges to 1 in the continuum limit. We perform the continuum extrapolation in three possible ways: without this improvement, with the tree-level improvement, and with the improvement factor of the free energy, that we find empirically to also reduce the cut-off effects at intermediate temperatures. We must then judge for every observable separately whether we can include the $N_t = 8$ and $N_t = 10$ ensembles, and which non-linear models are plausible and match the data. We have given examples for this in Fig. 4, but very often we simply add the models $A/(1 + B/N_t^2)$ and $A + B/N_t^2 + C/N_t^4$ to the linear fit.

We treat every mentioned option independently and perform 16–32 analyses per temperature, depending on the complexity of the continuum scaling. We use this large set of analyses to estimate the systematic errors temperature by temperature using the histogram method introduced in Refs. [85, 86]. In this paper we build a histogram of the results. The analyses with a fixed data set but different systematics are weighted using the Akaike Information Criterion (AIC) [87]. The AIC weigted results corresponding to the various fit windows in $1/N_t^2$ are combined with uniform weights. In the case of the charm susceptibility we calculate the systematic errors on the finite N_t points

first and then perform various continuum extrapolations which then enter the histogram method. Since all analyses are equally we identify the median with the result. The distribution of results is not necessarily Gaussian and may contain isolated combinations of the analysis options that produce outliers. These do not contribute to the median. The systematic error is the spread of the distribution. Instead of the standard deviation we use the spread of central 68% of the distribution, so that we do not have to make assumptions on the tail of the distribution. The median can be calculated for every jackknife or bootstrap sample. We use the variance of the median as statistical error. In the plots we show the combined errors, by adding up the systematic and statistical errors in quadrature.

IV. RESULTS IN THE CROSS-OVER REGION

Previous works have suggested that the Hadron Resonance Gas (HRG) model provides a good description of the data in the range 130-150 MeV [4, 36, 37, 44, 45], and perhaps missing strange resonances might account for the small deviations in the strangeness sector [88].

In this paper we supplement the picture with additional continuum extrapolated data. Finite lattice spacing studies (with or without a well improved action) can never state with certainty whether deviations from the model are a genuine effect. Here we compare our lattice results using the 2014 edition of the Particle Data Book [89].

In our previous paper [37] we have calculated nearly all the second order fluctuations. Only the most difficult correlator was omitted $\chi_{11}^{ud}(T)$, which is not only noisy but had severe lattice spacing effects, similar to $\chi_2^Q(T)$ in Fig. 4.
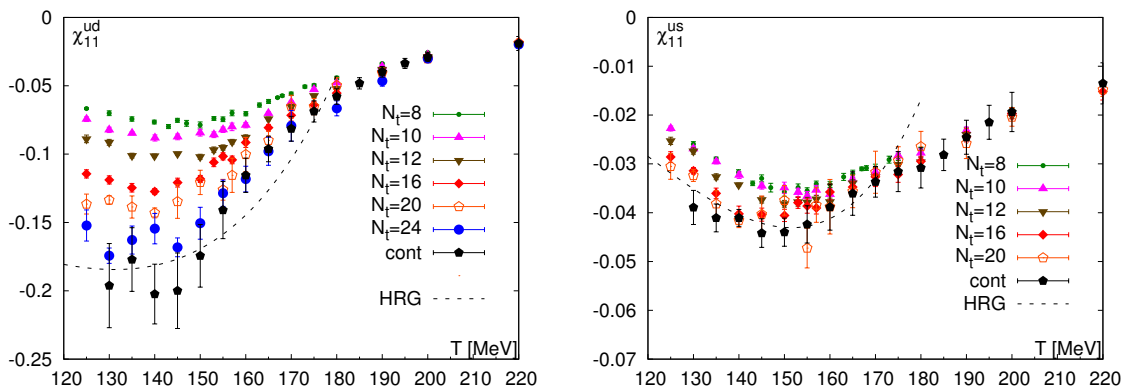

FIG. 6. The up-down correlator (χ_{11}^{ud}) and up-strange correlator (χ_{11}^{us}) for several lattice spacings and in the continuum limit. For the Hadron Resonance Gas model we use the resonance table in the 2014 edition of the Particle Data Book [89].

The continuum extrapolation of $\chi_{11}^{ud}(T)$ and the data in the full lattice spacing range are shown in Fig. 6, together with the up-strange correlator $\chi_{11}^{us}(T)$. The continuum limit for $\chi_{11}^{ud}(T)$ is well described by the HRG model up to $T \approx 155$ MeV, which lies at the centre of the transition region [4, 5]. The main hadrons that contribute to the HRG prediction are the light mesons, mostly pions (the combination of a quark with an anti-quark makes the χ_{11}^{ud} contribution negative). At high temperatures, heavier hadrons and their resonances have non-negligible Boltzmann factors, allowing the baryons (mostly protons) to take over the main role and bend the curve upwards. The important role played by the pions is also highlighted by the staggered lattice artefacts (taste breaking) that increase the mass of the various staggered pion-like degrees of freedom (tastes) [90]. Looking at Eq. (18) the discretization uncertainties in χ_{11}^{ud} mostly come from the χ_2^Q term, shown in the right panel of Fig. 4, they are eliminated by using fine lattices up to $N_t = 24$. There is no contribution to χ_{11}^{us} from χ_2^Q (see Eq. (19)), and the discretization errors are smaller, as expected (see Fig. 5). For χ_{11}^{ud} the strange resonances play no role. For χ_{11}^{us} any discrepancy between HRG and the strange susceptibilities [88] is minimized since χ_{11}^{us} is less sensitive to multi-strange contributions and the corresponding HRG now includes all relevant resonances from PDG-2014 [89].

In lattice QCD $\chi_{11}^{ud}(T) \sim \langle A_u A_d \rangle /V$ in Eq. (35)'s notation. The $A = (1/4)\mathrm{Tr}M^{-1}M'$ operator is a trace over the whole lattice. The normalized Gaussian random sources (χ) that we use to evaluate A, contribute each as $\chi^+ M^{-1}M'\chi/4 \sim V$. This C-odd estimator is widely oscillating between sources. Thus, in A and then also in the stochastic representation of $\langle AA \rangle /V$, large cancellations occur between opposite-sign contributions. Refs. [26, 91] link the phase of the fermion determinant at small μ_B to the odd operators A and C. Indeed, the sign problem is already present in the Taylor-expansion technique and in the calculation of baryonic fluctuations in general.

The consequence is that the severity of the sign problem is related to the magnitude of χ_{11}^{ud}. In early staggered studies one saw peak heights of ≈ -0.005 [26], ≈ -0.014 [29], and ≈ -0.05 [27], are well short of today's continuum limit in Fig. 6. With the early actions and coarse lattices the calculation of higher derivatives and reweighting were easier.

Note that the light isospin susceptibility (χ_2^I) does not depend on the A operator, $\chi_2^I \sim \langle B \rangle$, it does not contain any disconnected diagrams at all. The fourth derivative $\chi_4^I \sim [6 \langle \delta B^2 \rangle - \langle D \rangle]/V$, too, contains only C-even operators. Indeed, thermodynamics at finite isospin chemical potential is not plagued by the sign problem.
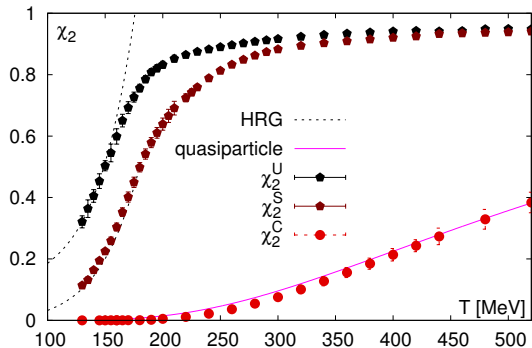

FIG. 7. Light, strange and charm diagonal quark number susceptibilities in the continuum limit as functions of the temperature. The quasi-particle model is calculated for a single, non-interacting charm quark with a fitted mass $m_c^{\mathrm{QP}} = 1430$ MeV.

A subset of the authors of this paper have remarked that one can observe a hierarchy between flavors in their fluctuations [39]. We are now extending the picture and show the continuum extrapolations of the flavor-specific quark number susceptibilities in Fig. 7. The HRG model describes the light flavors reasonably well. The charm susceptibility in Fig. 7 rises at higher temperatures, compared to the lighter flavors. It was emphasized in Ref. [92] that open charm with fractional baryon charge starts appearing near the chiral crossover temperature. In addition to the hadron resonance gas model we show a naive quasiparticle estimate for the charm susceptibility (see also [93]). The mass of the charm quark was fitted to the last points $(m_c^{\mathrm{QP}} = 1430$ MeV). This mass is empirical, and may depend on the range of the matching to our lattice data. In general the mass of the charm quark is scheme dependent. The susceptibility curve runs near the quasiparticle model, qualitatively confirming that χ_2^C is contributed to by the deconfined charm quark. Nevertheless, the quasiparticle model's results are overestimating the lattice data below approx. 350 MeV. This leaves room for multiple interpretations (e.g. T-dependent m_c^{QP}, limitations of the quasiparticle model or charmonium bound states that absorb some of the free quarks).

Figures 8 and 9 detail our continuum results for the fourth order cumulants. The normalized strangeness (χ_4^S/χ_2^S) [39] and baryon cumulants (χ_4^B/χ_2^B) [19, 46] have been published in earlier works. In these publications we found that baryon ration was in agreement with HRG up to ≈ 145 MeV, whereas for the strange ratio a consistency was observed at up to 10-15 MeV higher temperatures.

In this paper we show the fourth derivative with respect to the light single quark chemical potential (Fig. 8). On coarse lattices we see a strong peak around the transition temperature.

Such a peak has indeed been expected: if QCD is in the chiral scaling regime with an $O(N)$ symmetry (i.e. the light quark masses are small enough for QCD being nearly chiral) then this scaling is expected to dominate the so called magnetic equation of state [94], which parametrizes the singular part of the free energy as a reduced temperature and the quark masses that play the role of the magnetic field in the $O(N)$ model's language. The chemical potential enters through its shifting effect on the transition temperature. At finite μ, the reduced temperature is $t \sim (T - T_c)/T_c - \kappa \mu^2/T^2$, where κ is the curvature of the QCD transition line [95]. Using the critical exponents one has, for the n-th derivative, a singular contribution of $\chi_n^B \sim |t|^{2-\alpha-n/2}$, with $2 - \alpha = \beta\delta(1 + 1/\delta)$ [96]. In the $O(4)$ universality class $\alpha = -0.2131(34)$ [97]. The non-analytic contribution of $\chi_4^B(T)$ is thus singular in the chiral limit and has a mild peak near T_c at finite mass, while $\chi_6^B(T)$ changes sign near T_c [96].

The data in Fig. 8 show that the peak is strongly reduced on finer lattices, as if we were moving away from the chiral limit. It will be interesting to see if this pattern is observed with other actions with an improved dispersion relation. Since here the $N_t = 24$ data have insufficient statistics, we cannot perform a controlled continuum extrapolation at all temperatures: we call our result below T_c a continuum estimate. What we see is that already at 145 MeV the Hadron Resonance Gas model is unlikely to describe the lattice data. From our extrapolation based on $N_t = 8, 10, 12$
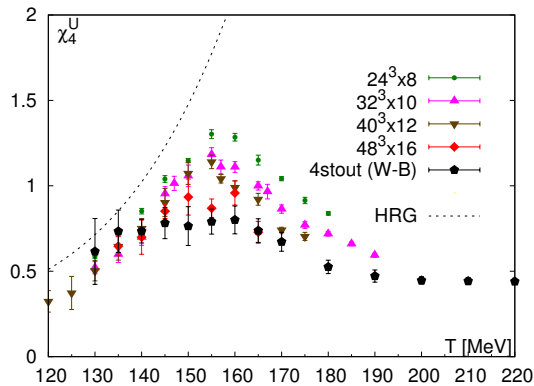
FIG. 8. The single light quark number fourth order susceptibility in the cross-over region. The extrapolation is driven by the $LT = 3$ set of ensembles, which are plotted together with the extrapolation and the HRG prediction. (From $T > 165$ MeV the continuum extrapolation uses only the $LT = 4$ lattices (not shown)). Since this is a potentially pion-driven observable and the $N_t = 24$ data are not sufficiently precise, the extrapolation is based on $N_t = 8 \dots 20$ lattices. In the cross-over region we consider this a continuum estimate only.

and 16 lattices it is plausible to assume agreement at 135 MeV.
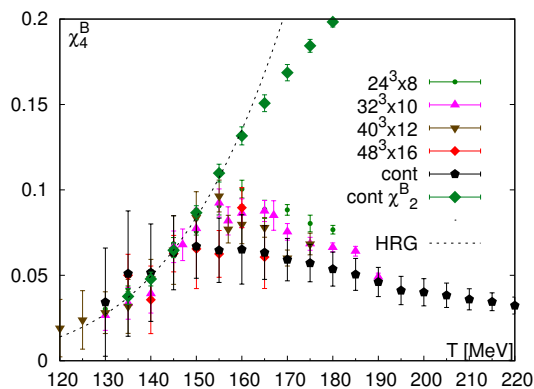

FIG. 9. Continuum limit of the fourth moment of the baryon number distribution. We also show the second moment. The HRG model gives the same result for the two observables. The departure of χ_4^B from χ_2^B was interpreted as a signal of deconfinement in Ref. [46].

The baryon fourth moment shows milder lattice artefacts; here the large statistical errors dominate over the systematic errors (see Fig. 9). We also show $\chi_2^B(T)$ since the second and fourth moment receive the same prediction from the HRG model, independently of how many baryons and mesons are included in the resonance list. The point where $\chi_2^B(T)$ and $\chi_4^B(T)$ are no longer consistent cannot be described by any resonance list. Multi-baryon states are expected to lead to $\chi_4^B > \chi_2^B$, but here we observe the opposite from $T > 155$ MeV. The relation $\chi_4^B < \chi_2^B$ motivates the concept that the free energy is dominated by objects with fractional baryon numbers: quarks. Given the trend of the HRG model, it is conceivable that the departure point from the HRG model, and the respective maximum of the fourth-order derivative (χ_4^U or χ_4^B) are very close in temperature.

V. RESULTS AT HIGH TEMPERATURES

In this section we show our continuum extrapolated results at intermediate and high temperatures. The first observables are the off-diagonal quark flavor correlators, already shown in the transition region in Fig. 6. Increasing the temperature range (see Fig. 10), we actually see that the value of the light-light correlator spans more than two orders of magnitude between T_c and $5T_c$. Between $4T_c$ and $5T_c$ the leading perturbative log, which was calculated at

zero quark mass [62], describes our data. The mass of the strange quark is negligible in this observable already at a temperature $\sim$240 MeV. Our data suggest that the light-charm correlator becomes compatible with the light-light correlator at about $4T_c$, but its agreement with the leading log starts a bit earlier. According to these data the charm quark decouples at intermediate and high temperature from the rest in alignment with the perturbative expectations. This is consistent with the nearly quasi-particle behaviour of the charm quark in the diagonal fluctuation χ_2^C.
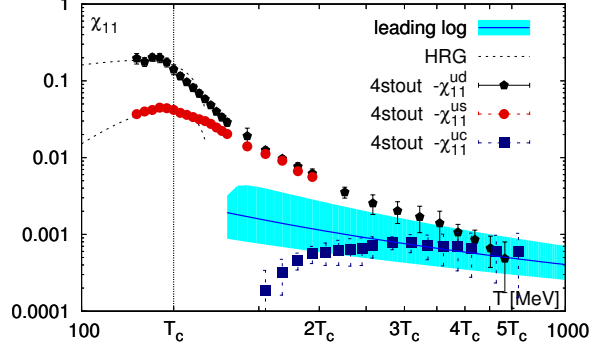

FIG. 10. The off-diagonal quark number susceptibilities for various flavor combinations (see also Fig. 6). The light correlator spans more than two orders of magnitude in the temperature range between T_c and $5T_c$ (using the rescaling factor $T_c = 155$ MeV). The leading $\mathcal{O}(\alpha^3 \log \alpha)$ perturbative result is from Ref. [62]. The mass of the strange quark becomes irrelevant near $1.5T_c$. At $3T_c$ even the charm quark correlator agrees with the perturbative result, even though the latter was calculated at zero mass.

For the light quark number susceptibility (Fig. 11) there are continuum results available [37, 40]. Here we compare to the recent result with the HISQ action (with a combined analysis also using p4 data) [40]. Our result is compatible with both Refs. [37, 40] within errorbars. Here we also show the latest (improved) perturbative estimates, based on hard thermal loops (HTL) [61] and dimensional reduction (DR) [52]. The improvement used in Ref. [52] has reduced the renormalization scale dependence enormously. Our data are approximately one sigma higher than the upper edge of the yellow band of the DR result. The central line of the band is calculated at the renormalization scale $2\pi T$, the upper edge at $4\pi T$ and the lower edge at πT.
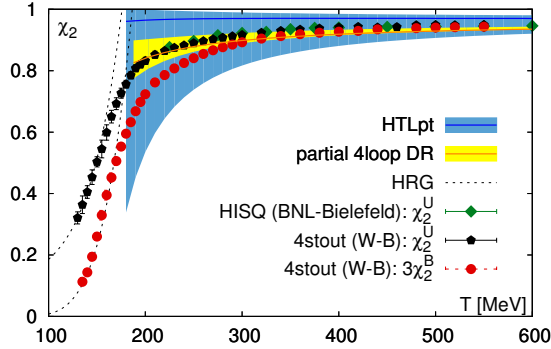

FIG. 11. Second order diagonal fluctuations using the single quark chemical potential χ_2^U vs. the baryon chemical potential χ_2^B; we also compare our data to the BNL-Bielefeld result [40].

The fourth order cumulants at high and intermediate temperature are shown in Fig. 12. Both χ_4^U and χ_4^B are the fourth derivative of the free energy with respect to the chemical potential, the difference is that for the former the chemical potential is associated with only one of the quarks, whereas for the latter it is associated with all quarks at the same time. Here the HTL results have a very small renormalization scale dependence. The data confirms the HTL prediction that the Stefan-Boltzmann limit is (almost) reached for χ_4^B at intermediate temperatures, χ_4^U approaches

it much slower. In both cases the improved and resummed perturbative results give an accurate description of lattice data above 250 MeV.

This agreement may seem trivial since the lattice result is continuum extrapolated and resummed perturbation theory is evaluated at high temperatures, both approaches are expected to solve QCD. There is a subtle difference, however, between HTL theory and lattice solutions. We simulated our ensembles with physical quark masses and 2+1+1 dynamical flavors. HTL results, on the other hand, are available for massless quarks only, and for $N_f = 3$ as well as for $N_f = 4$. The mass of the strange quarks becomes irrelevant before we see agreement between lattice data and HTL. At intermediate temperatures the large mass of the charm makes the $N_f = 3$ Hard Thermal Loop theory the closest match to our setting. In order to compare the same observables we do not count the baryon charge of the charm quark in χ_4^B and χ_2^B. To estimate the effect of the charm quark in the sea from the improved perturbation theory side we plot the three-flavor and four-flavor result for χ_4^U together in Fig. 12 (see Ref. [64]).
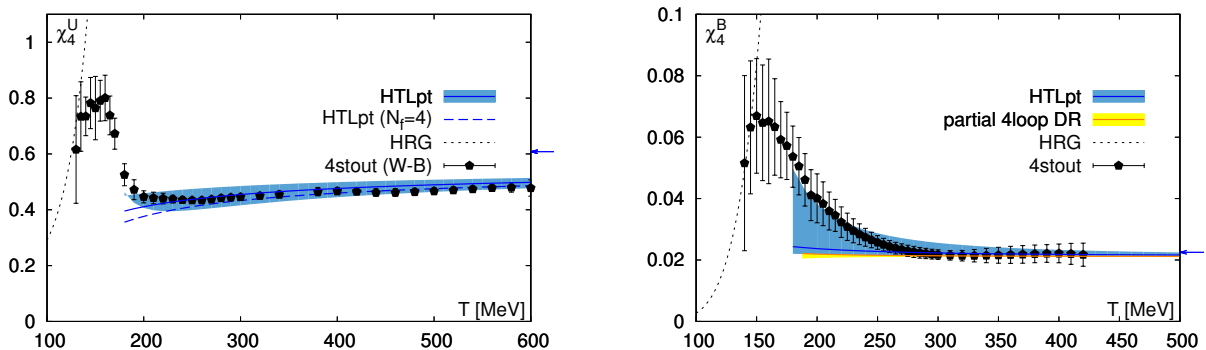

FIG. 12. Fourth order cumulants from our lattice study versus hard thermal loops [64] and the result from dimensional reduction (DR) [52]. The small arrows on the right hand side mark the Stefan-Boltzmann limit.

We close our discussion with the off-diagonal fourth order correlator. In Fig. 13 we show both the light-light and the light-strange correlator. Here the effect of the strange quark mass diminishes even sooner, at around 200 MeV. The agreement with the HTL result starts at a temperature $T \sim 250$ MeV, in accordance with the other observables We also show the prediction of dimensional reduction [52].
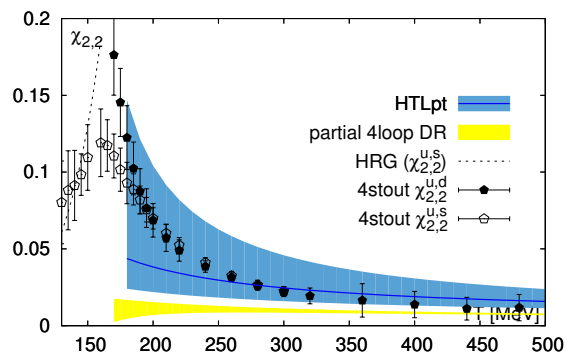
FIG. 13. The off-diagonal fourth order fluctuation at high temperature. Only this off-diagonal derivative has a non-vanishing contribution in three-loop HTL [64]. The mass of the strange quark is irrelevant from approx. 200 MeV. Although the renormalization scale dependence between πT and $4\pi T$ is large enough to contain the data, an agreement with the central line and with its trend in temperature is reached at about 270 MeV. The prediction of the DR method is also shown [52], there is slight disagreement to HTL. Our data is compatible with both at high temperature.

VI. CONCLUDING REMARKS

In this paper we introduced our thermodynamics program with the four-level-smeared (4stout) staggered action. We focused on the fluctuations of conserved charges and updated our earlier result on second order fluctuations [37]. Since our first paper on fluctuations, we have introduced very fine lattices ($N_t = 24$) in the transition range and extended the analysis to high temperatures where a comparison to resummed and improved perturbation theory is possible. We have also presented diagonal and off-diagonal fourth order cumulants. Here our data could be used to determine the lowest temperature for the three-loop HTL approximation: approx. 250 MeV.

We have studied whether the hadron resonance gas (HRG) model gives an adequate description of the fluctuation data. We find that well below the deconfinement temperature, i.e. around 130 MeV, all studied observables are well described by the HRG model. This was the most difficult to demonstrate for the fourth moment of the net charge distribution χ_Q^4, which is a candidate for the freeze-out thermometer at the LHC. In this case, after adding a $96^3 \times 32$ lattice to the analysis ($a = 0.047$ fm), our continuum extrapolation based on $N_t = 20$, 24 and 32 lattices is consistent with the HRG model prediction.

It is very likely that HRG does not describe *all* aspects of fluctuations in QCD thermodynamics below the transition. But for quantities for which it does one can introduce the highest temperature of agreement between lattice and HRG. This indicator of deconfinement is unavoidably model-dependent, even if one considers combinations that do not or only weakly depend on the actual list of resonances. This temperature can, however, be determined as long as the continuum limits are feasible with a sufficient precision. The data on our plots show in most cases an agreement up to $\sim T_c$, which can move to a lower temperature as our precision improves. This should not be confused with the limiting temperature of the Hagedorn spectrum, which can be higher. The temperature of highest agreement is not the same for all fluctuations as it was also suggested in Ref. [39], e.g. χ_4^U and very possibly χ_4^Q depart from the HRG estimates at lower temperatures. This may be a signal of the limitations of the HRG approach, but also suggests that the transition is a broad cross-over.

VII. ACKNOWLEDGMENTS

Appendix A: Continuum results

We tabulate the presented continuum extrapolated results in this appendix. The diagonal and off-diagonal quark number fluctuations are shown to second order in Table. III and fourth order in Table. IV.

Appendix B: Simulation parameters

In this appendix we provide a list of simulation parameters for an extensive set the used runs (table V). The temperatures refer to the f_π scale setting method. We give the tentative values and remind the reader, that the actual scale at the given parameter has systematic errors that we propagate into the final results. For each lattice spacing and temperature we give inverse coupling β, the light and strange bare quark masses (m_{ud}, m_s). The charm quark mass can be calculated through $m_c = 11.85 m_s$. In cases where we had different volumes the bare parameters

were identical. We tabulate the parameters for up to $N_t = 16$, for the finer lattices with lower temperatures the parameters can be easily calculated.

***

[1] Y. Aoki, G. Endrodi, Z. Fodor, S. Katz, and K. Szabo, Nature **443**, 675 (2006), arXiv:hep-lat/0611014 [hep-lat].
[2] Y. Aoki, Z. Fodor, S. Katz, and K. Szabo, Phys.Lett. **B643**, 46 (2006), arXiv:hep-lat/0609068 [hep-lat].
[3] Y. Aoki, S. Borsanyi, S. Durr, Z. Fodor, S. D. Katz, *et al.*, JHEP **0906**, 088 (2009), arXiv:0903.4155 [hep-lat].
[4] S. Borsanyi *et al.* (Wuppertal-Budapest Collaboration), JHEP **1009**, 073 (2010), arXiv:1005.3508 [hep-lat].
[5] A. Bazavov, T. Bhattacharya, M. Cheng, C. DeTar, H. Ding, *et al.*, Phys.Rev. **D85**, 054503 (2012), arXiv:1111.1710 [hep-lat].
[6] S. Jeon and V. Koch, Phys.Rev.Lett. **85**, 2076 (2000), arXiv:hep-ph/0003168 [hep-ph].
[7] M. Asakawa, U. W. Heinz, and B. Muller, Phys.Rev.Lett. **85**, 2072 (2000), arXiv:hep-ph/0003169 [hep-ph].
[8] X. Luo, J.Phys.Conf.Ser. **599**, 012023 (2015), arXiv:1501.03010 [nucl-ex].
[9] M. A. Stephanov, K. Rajagopal, and E. V. Shuryak, Phys.Rev. **D60**, 114028 (1999), arXiv:hep-ph/9903292 [hep-ph].
[10] F. Karsch and K. Redlich, Phys.Lett. **B695**, 136 (2011), arXiv:1007.2581 [hep-ph].
[11] F. Becattini, J. Manninen, and M. Gazdzicki, Phys.Rev. **C73**, 044905 (2006), arXiv:hep-ph/0511092 [hep-ph].
[12] J. Cleymans, H. Oeschler, K. Redlich, and S. Wheaton, Phys.Rev. **C73**, 034905 (2006), arXiv:hep-ph/0511094 [hep-ph].
[13] A. Andronic, P. Braun-Munzinger, and J. Stachel, Nucl.Phys. **A772**, 167 (2006), arXiv:nucl-th/0511071 [nucl-th].
[14] A. Andronic, P. Braun-Munzinger, and J. Stachel, Phys.Lett. **B673**, 142 (2009), arXiv:0812.1186 [nucl-th].
[15] F. Becattini, M. Bleicher, E. Grossi, J. Steinheimer, and R. Stock, (2014), arXiv:1405.0710 [nucl-th].
[16] L. Adamczyk *et al.* (STAR Collaboration), Phys.Rev.Lett. **112**, 032302 (2014), arXiv:1309.5681 [nucl-ex].
[17] L. Adamczyk *et al.* (STAR Collaboration), Phys.Rev.Lett. **113**, 092301 (2014), arXiv:1402.1558 [nucl-ex].
[18] A. Bazavov, H. Ding, P. Hegde, O. Kaczmarek, F. Karsch, *et al.*, Phys.Rev.Lett. **109**, 192302 (2012), arXiv:1208.1220 [hep-lat].
[19] S. Borsanyi, Z. Fodor, S. Katz, S. Krieg, C. Ratti, *et al.*, Phys.Rev.Lett. **111**, 062005 (2013), arXiv:1305.5161 [hep-lat].
[20] S. Borsanyi, Z. Fodor, S. Katz, S. Krieg, C. Ratti, *et al.*, Phys.Rev.Lett. **113**, 052301 (2014), arXiv:1403.4576 [hep-lat].
[21] S. A. Gottlieb, W. Liu, D. Toussaint, R. Renken, and R. Sugar, Phys.Rev.Lett. **59**, 2247 (1987).
[22] S. A. Gottlieb, W. Liu, D. Toussaint, R. Renken, and R. Sugar, Phys.Rev. **D38**, 2888 (1988).
[23] R. Gavai, J. Potvin, and S. Sanielevici, Phys.Rev. **D40**, 2743 (1989).
[24] R. V. Gavai, S. Gupta, and P. Majumdar, Phys.Rev. **D65**, 054506 (2002), arXiv:hep-lat/0110032 [hep-lat].
[25] R. V. Gavai and S. Gupta, Phys.Rev. **D67**, 034501 (2003), arXiv:hep-lat/0211015 [hep-lat].
[26] C. Allton, S. Ejiri, S. Hands, O. Kaczmarek, F. Karsch, *et al.*, Phys.Rev. **D66**, 074507 (2002), arXiv:hep-lat/0204010 [hep-lat].
[27] C. Bernard *et al.* (MILC Collaboration), Phys.Rev. **D71**, 034504 (2005), arXiv:hep-lat/0405029 [hep-lat].
[28] R. Gavai and S. Gupta, Phys.Rev. **D73**, 014004 (2006), arXiv:hep-lat/0510044 [hep-lat].
[29] C. Allton, M. Doring, S. Ejiri, S. Hands, O. Kaczmarek, *et al.*, Phys.Rev. **D71**, 054508 (2005), arXiv:hep-lat/0501030 [hep-lat].
[30] S. Datta, R. V. Gavai, and S. Gupta, Nucl.Phys. **A904-905**, 883c (2013), arXiv:1210.6784 [hep-lat].
[31] S. Borsanyi, S. Durr, Z. Fodor, C. Hoelbling, S. D. Katz, *et al.*, JHEP **1208**, 126 (2012), arXiv:1205.0440 [hep-lat].
[32] S. Borsanyi, S. Durr, Z. Fodor, C. Holbling, S. D. Katz, *et al.*, (2015), arXiv:1504.03676 [hep-lat].
[33] P. Giudice, G. Aarts, C. Allton, A. Amato, S. Hands, *et al.*, PoS **LATTICE2013**, 492 (2014), arXiv:1309.6253 [hep-lat].
[34] G. Aarts, C. Allton, A. Amato, P. Giudice, S. Hands, *et al.*, JHEP **1502**, 186 (2015), arXiv:1412.6411 [hep-lat].
[35] C. Gattringer and H.-P. Schadler, Phys.Rev. **D91**, 074511 (2015), arXiv:1411.5133 [hep-lat].
[36] A. Bazavov *et al.* (HotQCD Collaboration), Phys.Rev. **D86**, 034509 (2012), arXiv:1203.0784 [hep-lat].
[37] S. Borsanyi, Z. Fodor, S. D. Katz, S. Krieg, C. Ratti, *et al.*, JHEP **1201**, 138 (2012), arXiv:1112.4416 [hep-lat].
[38] S. Borsanyi, Nucl.Phys. **A904-905**, 270c (2013), arXiv:1210.6901 [hep-lat].
[39] R. Bellwied, S. Borsanyi, Z. Fodor, S. D. Katz, and C. Ratti, Phys.Rev.Lett. **111**, 202302 (2013), arXiv:1305.6297 [hep-lat].
[40] A. Bazavov, H.-T. Ding, P. Hegde, F. Karsch, C. Miao, *et al.*, Phys.Rev. **D88**, 094021 (2013), arXiv:1309.2317 [hep-lat].
[41] R. Dashen, S.-K. Ma, and H. J. Bernstein, Phys.Rev. **187**, 345 (1969).
[42] R. Venugopalan and M. Prakash, Nucl.Phys. **A546**, 718 (1992).
[43] F. Karsch, K. Redlich, and A. Tawfik, Phys.Lett. **B571**, 67 (2003), arXiv:hep-ph/0306208 [hep-ph].
[44] P. Huovinen and P. Petreczky, Nucl.Phys. **A837**, 26 (2010), arXiv:0912.2541 [hep-ph].
[45] S. Borsanyi, Z. Fodor, C. Hoelbling, S. D. Katz, S. Krieg, *et al.*, Phys.Lett. **B730**, 99 (2014), arXiv:1309.5258 [hep-lat].
[46] A. Bazavov, H. T. Ding, P. Hegde, O. Kaczmarek, F. Karsch, *et al.*, Phys. Rev. Lett. 111, **082301**, 082301 (2013), arXiv:1304.7220 [hep-lat].
[47] K. Kajantie, M. Laine, K. Rummukainen, and Y. Schroder, Phys.Rev. **D67**, 105008 (2003), arXiv:hep-ph/0211321 [hep-ph].
[48] A. Vuorinen, Phys.Rev. **D68**, 054017 (2003), arXiv:hep-ph/0305183 [hep-ph].
[49] A. Vuorinen, Phys.Rev. **D67**, 074032 (2003), arXiv:hep-ph/0212283 [hep-ph].
[50] J. Blaizot, E. Iancu, and A. Rebhan, Phys.Rev. **D68**, 025011 (2003), arXiv:hep-ph/0303045 [hep-ph].
[51] J. O. Andersen, S. Mogliacci, N. Su, and A. Vuorinen, Phys.Rev. **D87**, 074003 (2013), arXiv:1210.0912 [hep-ph].

[52] S. Mogliacci, J. O. Andersen, M. Strickland, N. Su, and A. Vuorinen, JHEP **1312**, 055 (2013), arXiv:1307.8098 [hep-ph].
[53] E. Braaten and R. D. Pisarski, Phys.Rev. **D45**, 1827 (1992).
[54] J. O. Andersen, E. Braaten, E. Petitgirard, and M. Strickland, Phys.Rev. **D66**, 085016 (2002), arXiv:hep-ph/0205085 [hep-ph].
[55] J. O. Andersen, M. Strickland, and N. Su, JHEP **1008**, 113 (2010), arXiv:1005.1603 [hep-ph].
[56] G. Boyd, J. Engels, F. Karsch, E. Laermann, C. Legeland, *et al.*, Nucl.Phys. **B469**, 419 (1996), arXiv:hep-lat/9602007 [hep-lat].
[57] S. Borsanyi, G. Endrodi, Z. Fodor, S. Katz, and K. Szabo, JHEP **1207**, 056 (2012), arXiv:1204.6184 [hep-lat].
[58] M. Strickland, J. O. Andersen, L. E. Leganger, and N. Su, Prog.Theor.Phys.Suppl. **187**, 106 (2011), arXiv:1011.0416 [hep-ph].
[59] J. O. Andersen, L. E. Leganger, M. Strickland, and N. Su, Phys.Rev. **D84**, 087703 (2011), arXiv:1106.0514 [hep-ph].
[60] N. Haque, M. G. Mustafa, and M. Strickland, JHEP **1307**, 184 (2013), arXiv:1302.3228 [hep-ph].
[61] N. Haque, J. O. Andersen, M. G. Mustafa, M. Strickland, and N. Su, Phys.Rev. **D89**, 061701 (2014), arXiv:1309.3968 [hep-ph].
[62] J. Blaizot, E. Iancu, and A. Rebhan, Phys.Lett. **B523**, 143 (2001), arXiv:hep-ph/0110369 [hep-ph].
[63] J. Blaizot, E. Iancu, and A. Rebhan, Eur.Phys.J. **C27**, 433 (2003), arXiv:hep-ph/0206280 [hep-ph].
[64] N. Haque, A. Bandyopadhyay, J. O. Andersen, M. G. Mustafa, M. Strickland, *et al.*, JHEP **1405**, 027 (2014), arXiv:1402.6907 [hep-ph].
[65] A. Bzdak, V. Koch, and V. Skokov, Phys.Rev. **C87**, 014901 (2013), arXiv:1203.4529 [hep-ph].
[66] V. Skokov, B. Friman, and K. Redlich, Phys.Rev. **C88**, 034911 (2013), arXiv:1205.4756 [hep-ph].
[67] P. Alba, R. Bellwied, M. Bluhm, V. M. Sarti, M. Nahrgang, *et al.*, (2015), arXiv:1504.03262 [hep-ph].
[68] J. I. Kapusta and C. Gale, *Finite-Temperature Field Theory*, 2nd ed. (Cambridge University Press, 2006) cambridge Books Online.
[69] T. Toimela, Phys.Lett. **B124**, 407 (1983).
[70] P. Hasenfratz and F. Karsch, Phys.Lett. **B125**, 308 (1983).
[71] O. Kaczmarek, C. Schmidt, P. Steinbrecher, and M. Wagner, (2014), arXiv:1411.4439 [physics.comp-ph].
[72] G. S. Bali, S. Collins, and A. Schafer, Comput.Phys.Commun. **181**, 1570 (2010), arXiv:0910.3970 [hep-lat].
[73] C. Morningstar and M. J. Peardon, Phys.Rev. **D69**, 054501 (2004), arXiv:hep-lat/0311018 [hep-lat].
[74] C. Davies, C. McNeile, K. Wong, E. Follana, R. Horgan, *et al.*, Phys.Rev.Lett. **104**, 132003 (2010), arXiv:0910.3102 [hep-ph].
[75] S. Aoki *et al.*, Eur. Phys. J. **C74**, 2890 (2014), arXiv:1310.8555 [hep-lat].
[76] J. L. Rosner and S. Stone, (2013), arXiv:1309.1924 [hep-ex].
[77] S. Borsanyi, S. Dürr, Z. Fodor, *et al.*, "Determination of f_k/f_π from 2+1+1 flavor 4-stout staggered lattices," (2015), (in preparation).
[78] C. McNeile, C. Davies, E. Follana, K. Hornbostel, and G. Lepage, Phys.Rev. **D82**, 034512 (2010), arXiv:1004.4285 [hep-lat].
[79] S. Durr, Z. Fodor, C. Hoelbling, S. Katz, S. Krieg, *et al.*, Phys.Lett. **B701**, 265 (2011), arXiv:1011.2403 [hep-lat].
[80] S. Durr, Z. Fodor, C. Hoelbling, S. Katz, S. Krieg, *et al.*, JHEP **1108**, 148 (2011), arXiv:1011.2711 [hep-lat].
[81] S. Borsanyi, S. Durr, Z. Fodor, S. Krieg, A. Schafer, *et al.*, Phys.Rev. **D88**, 014513 (2013), arXiv:1205.0788 [hep-lat].
[82] S. Borsanyi, S. Durr, Z. Fodor, C. Hoelbling, S. D. Katz, *et al.*, JHEP **1209**, 010 (2012), arXiv:1203.4469 [hep-lat].
[83] M. Luscher, JHEP **1008**, 071 (2010), arXiv:1006.4518 [hep-lat].
[84] S. Borsanyi, G. Endrodi, Z. Fodor, A. Jakovac, S. D. Katz, *et al.*, JHEP **1011**, 077 (2010), arXiv:1007.2580 [hep-lat].
[85] S. Durr, Z. Fodor, J. Frison, C. Hoelbling, R. Hoffmann, *et al.*, Science **322**, 1224 (2008), arXiv:0906.3599 [hep-lat].
[86] S. Borsanyi, S. Durr, Z. Fodor, C. Hoelbling, S. Katz, *et al.*, Science **347**, 1452 (2015), arXiv:1406.4088 [hep-lat].
[87] H. Akaike, IEEE Transactions on Automatic Control **19** (1974).
[88] A. Bazavov, H. T. Ding, P. Hegde, O. Kaczmarek, F. Karsch, *et al.*, Phys.Rev.Lett. **113**, 072001 (2014), arXiv:1404.6511 [hep-lat].
[89] K. A. Olive *et al.* (Particle Data Group), Chin. Phys. **C38**, 090001 (2014).
[90] C. Bernard, M. Golterman, and Y. Shamir, Phys.Rev. **D73**, 114511 (2006), arXiv:hep-lat/0604017 [hep-lat].
[91] S. Ejiri, Phys.Rev. **D78**, 074507 (2008), arXiv:0804.3227 [hep-lat].
[92] A. Bazavov, H. T. Ding, P. Hegde, O. Kaczmarek, F. Karsch, *et al.*, Phys.Lett. **B737**, 210 (2014), arXiv:1404.4043 [hep-lat].
[93] P. Petreczky, P. Hegde, and A. Velytsky (RBC-Bielefeld Collaboration), PoS **LAT2009**, 159 (2009), arXiv:0911.0196 [hep-lat].
[94] S. Ejiri, F. Karsch, E. Laermann, C. Miao, S. Mukherjee, *et al.*, Phys.Rev. **D80**, 094505 (2009), arXiv:0909.5122 [hep-lat].
[95] O. Kaczmarek, F. Karsch, E. Laermann, C. Miao, S. Mukherjee, *et al.*, Phys.Rev. **D83**, 014504 (2011), arXiv:1011.3130 [hep-lat].
[96] B. Friman, F. Karsch, K. Redlich, and V. Skokov, Eur.Phys.J. **C71**, 1694 (2011), arXiv:1103.3511 [hep-ph].
[97] J. Engels, L. Fromme, and M. Seniuch, Nucl.Phys. **B675**, 533 (2003), arXiv:hep-lat/0307032 [hep-lat].
[98] V. Hernandez, J. E. Roman, and V. Vidal, ACM Trans. Math. Software **31**, 351 (2005).
[99] *JUQUEEN: IBM Blue Gene/Q Supercomputer System at the Jülich Supercomputing Centre*, Tech. Rep. 1 A1 (Jülich Supercomputing Centre, http://dx.doi.org/10.17815/jlsrf-1-18, 2015).

T MeV	χ_2^u	χ_2^s	χ_2^c	χ_2^B	χ_{11}^{ud}	χ_{11}^{us}	χ_{11}^{uc}
130	0.321(20)	0.114(10)	0.00004(20)		-0.196(30)	-0.0389(30)	
135	0.364(30)	0.132(10)	-0.00002(10)	0.0376(50)	-0.177(20)	-0.0411(30)	
140	0.405(20)	0.1640(70)	-0.00002(20)	0.0478(40)	-0.202(20)	-0.0411(20)	
145	0.453(20)	0.1943(70)	0.00005(20)	0.0647(40)	-0.200(30)	-0.0442(30)	
150	0.503(20)	0.2251(70)	0.00007(20)	0.0866(40)	-0.174(20)	-0.0440(30)	
155	0.545(30)	0.259(10)	0.00024(30)	0.1098(50)	-0.141(20)	-0.0424(40)	
160	0.599(30)	0.304(10)	0.00031(40)	0.1316(50)	-0.115(10)	-0.0389(50)	
165	0.650(20)	0.352(10)	0.00035(50)	0.1507(50)	-0.0962(90)	-0.0361(40)	
170	0.693(20)	0.402(20)	0.00058(70)	0.1686(50)	-0.0815(90)	-0.0337(30)	
175	0.727(20)	0.449(20)		0.1843(40)	-0.0687(80)	-0.0316(40)	
180	0.756(10)	0.498(20)	0.0005(10)	0.1983(30)	-0.0579(60)	-0.0308(40)	
185	0.785(10)	0.542(20)		0.2109(30)	-0.0482(40)	-0.0282(30)	
190	0.808(10)	0.579(20)	0.0018(10)	0.2228(30)	-0.0398(40)	-0.0245(30)	
195	0.821(10)	0.611(20)		0.2327(40)	-0.0336(40)	-0.0215(30)	
200	0.832(10)	0.639(20)	0.0048(20)	0.2411(40)	-0.0289(30)	-0.0194(40)	
210	0.852(10)	0.691(20)		0.2539(40)			
220	0.8646(90)	0.724(10)	0.0111(30)	0.2620(40)	-0.0191(50)	-0.0135(40)	
230	0.8747(80)	0.7591(90)		0.2692(40)			
240	0.8826(70)	0.7885(90)	0.0215(40)	0.2751(40)	-0.0125(10)		-0.00019(20)
250	0.8897(80)	0.8131(90)		0.2803(30)			
260	0.8963(80)	0.8329(90)	0.0361(70)	0.2849(30)	-0.0097(10)		-0.00032(20)
270	0.9023(80)	0.8489(90)		0.2889(30)			
280	0.9076(80)	0.8625(90)	0.0544(80)	0.2922(30)	-0.00766(90)		-0.00046(10)
290	0.9123(80)	0.8740(80)		0.2951(30)			
300	0.9165(80)	0.8828(90)	0.076(10)	0.2976(30)	-0.00621(90)		-0.00056(10)
320	0.9238(70)	0.8943(90)	0.101(10)	0.3015(20)			-0.00058(20)
340	0.9296(60)	0.9028(90)	0.128(20)	0.3043(30)			-0.00062(20)
360	0.9339(60)	0.9091(80)	0.156(20)	0.3063(30)			-0.00063(20)
380	0.9374(60)	0.9150(70)	0.185(20)	0.3079(30)			-0.00065(30)
400	0.9388(40)	0.9206(70)	0.214(20)	0.3090(30)	-0.00254(70)		-0.00071(20)
420	0.9408(40)	0.9249(70)	0.243(20)	0.3099(20)			
440	0.9427(50)	0.9327(70)	0.273(30)	0.3116(20)			-0.00078(10)
480	0.9451(60)	0.9368(60)	0.329(30)	0.3129(10)			-0.00079(20)
500	0.9462(60)	0.9383(50)		0.3134(10)	-0.00169(60)		
520	0.9471(50)	0.9409(60)	0.384(30)	0.3139(10)			-0.00072(30)
550	0.9481(40)	0.9409(40)		0.3144(10)	-0.00140(60)		

TABLE III. Diagonal and off-diagonal second order fluctuations.

T MeV	χ_4^u	χ_4^B	χ_{22}^{ud}	χ_{22}^{us}
130	0.62(20)	0.034(30)		0.080(30)
135	0.73(10)	0.051(40)		0.088(30)
140	0.735(70)	0.052(30)		0.091(20)
145	0.782(90)	0.063(20)		0.098(10)
150	0.76(10)	0.067(20)		0.110(20)
160	0.801(80)	0.065(20)		0.119(20)
165	0.738(70)	0.063(20)		0.117(20)
170	0.672(60)	0.059(10)	0.176(30)	0.110(10)
175		0.057(10)	0.145(20)	0.102(10)
180	0.525(40)	0.054(10)	0.122(20)	0.093(10)
185		0.0505(90)	0.102(20)	0.089(10)
190	0.472(40)	0.0461(90)	0.088(10)	0.0819(90)
195		0.0411(80)	0.077(10)	0.0755(80)
200	0.446(20)	0.0401(80)	0.069(10)	0.0699(70)
210	0.442(20)	0.0360(60)	0.0572(90)	0.0602(60)
220	0.440(20)	0.0323(50)	0.0489(70)	0.0524(50)
240	0.435(10)	0.0274(30)	0.0385(40)	0.0411(30)
260	0.4340(90)	0.0244(20)	0.0315(30)	0.0325(30)
280	0.442(10)	0.0226(20)	0.0263(30)	0.0265(30)
300	0.4459(80)	0.0218(20)	0.0222(30)	0.0223(30)
320	0.450(10)	0.0214(20)	0.0194(50)	
400	0.467(10)	0.0222(30)	0.0137(90)	
440	0.462(10)	0.0206(50)	0.0110(70)	
480	0.464(10)	0.0199(50)	0.0117(90)	
520	0.470(10)	0.0199(50)	0.014(10)	

TABLE IV. Diagonal and off-diagonal fourth order fluctuations.

$N_t = 8$							
T MeV	β	m_{ud}	m_s	T MeV	β	m_{ud}	m_s
130	3.5462	0.00321128	0.0906668	190	3.7009	0.00206126	0.0578245
135	3.5620	0.00305286	0.0861789	200	3.7219	0.00195400	0.0547049
140	3.5771	0.00291258	0.0822005	220	3.7613	0.00177052	0.0493658
145	3.5914	0.00278764	0.0786528	240	3.7978	0.00161742	0.0449454
150	3.6052	0.00267563	0.0754670	260	3.8319	0.00148677	0.0412196
155	3.6185	0.00257449	0.0725853	280	3.8639	0.00137390	0.0380367
160	3.6314	0.00248254	0.0699595	300	3.8942	0.00127565	0.0352876
165	3.6438	0.00239837	0.0675501	360	3.9759	0.00104649	0.0289221
170	3.6558	0.00232086	0.0653251	440	4.0687	0.00084070	0.0232297
175	3.6676	0.00224907	0.0632590	520	4.1479	0.00070103	0.0193696
180	3.6790	0.00218228	0.0613308	600	4.2171	0.00060056	0.0165936
$N_t = 10$							
T MeV	β	m_{ud}	m_s	T MeV	β	m_{ud}	m_s
$N_t = 12$							
T MeV	β	m_{ud}	m_s	T MeV	β	m_{ud}	m_s
130	3.7115	0.00200610	0.0562213	190	3.8716	0.00134807	0.0373123
135	3.7270	0.00192900	0.0539768	200	3.8942	0.00127565	0.0352876
140	3.7420	0.00185777	0.0519023	220	3.9366	0.00115049	0.0318053
145	3.7565	0.00179158	0.0499772	240	3.9759	0.00104649	0.0289221
150	3.7706	0.00172979	0.0481850	260	4.0126	0.00095897	0.0264999
155	3.7844	0.00167188	0.0465116	280	4.0470	0.00088446	0.0244394
160	3.7978	0.00161742	0.0449454	300	4.0793	0.00082036	0.0226675
165	3.8108	0.00156609	0.0434762	360	4.1661	0.00067294	0.0185935
170	3.8236	0.00151761	0.0420951	440	4.2637	0.00054210	0.0149782
175	3.8360	0.00147176	0.0407946	520	4.3466	0.00045357	0.0125321
180	3.8481	0.00142833	0.0395679	600	4.4189	0.00038977	0.0107694
$N_t = 16$							
T MeV	β	m_{ud}	m_s	T MeV	β	m_{ud}	m_s
130	3.8319	0.00148677	0.0412196	190	4.0007	0.00098655	0.0272628
135	3.8481	0.00142833	0.0395679	200	4.0243	0.00093284	0.0257769
140	3.8639	0.00137390	0.0380367	220	4.0687	0.00084070	0.0232297
145	3.8793	0.00132311	0.0366135	240	4.1098	0.00076470	0.0211291
150	3.8942	0.00127565	0.0352876	260	4.1479	0.00070103	0.0193696
155	3.9087	0.00123123	0.0340496	280	4.1836	0.00064698	0.0178762
160	3.9228	0.00118959	0.0328912	300	4.2171	0.00060056	0.0165936
165	3.9366	0.00115049	0.0318053	360	4.3067	0.00049393	0.0136472
170	3.9500	0.00111374	0.0307855	440	4.4075	0.00039914	0.0110281
175	3.9631	0.00107913	0.0298261	520	4.4932	0.00033474	0.0092488
180	3.9759	0.00104649	0.0289221	600	4.5681	0.00028815	0.0079615

TABLE V. Simulation parameters for various lattice resolutions. Note that we fixed $m_c = 11.85 m_s$.